EVALUATION OF Cr(VI) ADSORPTION CAPACITY IN AQUEOUS SOLUTION USING MATERIAL RECOVERED FROM STEEL SLAG

Hoang Le Phuong*

Thai Nguyen University of Technology, Thai Nguyen City, Vietnam

*Corresponding author: phuongqtn@tnut.edu.vn

(Received: February 28, 2025; Revised: March 12, 2025; Accepted: March 15, 2025)

DOI: 10.31130/ud-jst.2025.23(6A).012E

Abstract - Steel slag (SS), an industrial by-product, has been investigated as a cost-effective adsorbent for removing hexavalent chromium Cr(VI) from aqueous solutions. Unlike previous studies that primarily focused on conventional adsorbents, this research systematically investigates the adsorption behavior of SS, emphasizing its kinetic and isotherm characteristics. Batch experiments revealed that Cr(VI) adsorption reached equilibrium within 150 minutes under acidic conditions, with optimal performance at pH 3. Adsorption kinetics followed the pseudo-second-order model (R^2=0.985), indicating chemisorption dominance. The Langmuir isotherm provided the best fit (R^2=0.986), with a maximum adsorption capacity of 13.32 mg/g at an initial Cr(VI) concentration of 20 mg/L, suggesting monolayer adsorption on uniform sites. This study provides novel insights by demonstrating the effectiveness of SS as an alternative low-cost adsorbent that has not yet received specific attention in Vietnam. These findings confirm the feasibility of SS for Cr(VI) removal, contributing to environmentally friendly water treatment solutions.

Key words - Adsorption; Steel slag (SS); Cr(VI) removal

1. Introduction

Hexavalent chromium (Cr(VI)) is a highly toxic trace metal widely used in various industrial applications, including chromium mining, electroplating, leather tanning, dyeing, paper pigmentation, and photography [1]. Its presence in the environment poses significant threats to human health and ecosystems due to its teratogenic, carcinogenic, and mutagenic effects. The World Health Organization (WHO) has set a strict guideline, limiting the maximum permissible concentration of Cr(VI) in drinking water to less than 50 µg/L [2]. Consequently, effective and sustainable methods for Cr(VI) removal from wastewater are of paramount importance.

Various technologies have been developed to remove Cr(VI) contamination, such as membrane separation, chemical precipitation, electrocoagulation, ion exchange, biological processes, and adsorption. Among these, adsorption stands out for its high efficiency, low cost, and ease of operation [1, 3]. Identifying cost-effective adsorbents with high adsorption capacities is crucial for optimizing adsorption processes [4]. Many adsorbents have been successfully studied for Cr(VI) adsorption from wastewater such as thetic adsorbent (magnetic nanoparticles, Ppy- Fe_3O_4/rGO, $BaFe_{12}O_{19}$ magnetic nanopowder) [5–7]; natural organic (woody-activated carbon, grape waste, biochar from wheat straw) [8–10]; inorganic adsorbents (kaolin, clay-zeolite composite, red mud, fly ash, furnace slag) [11–15]. Compared to the materials mentioned above, inorganic adsorbents offer notable advantages, including superior chemical and mechanical strength as well as a high ion exchange capacity - key factors in effective adsorption processes for wastewater treatment [16]. Consequently, adsorbents derived from waste materials such as clay minerals, coal fly ash, blast furnace slag, and steel slag have garnered increasing interest due to their cost-effectiveness, widespread availability, and potential for secondary applications.

SS, a byproduct of the steel production process, accounts for approximately 15% of the total steel output by mass [17]. According to the Vietnam Steel Association, the country hosts over 70 factories producing crude and finished steel. In 2020, crude steel production reached an estimated 18 million tons, generating about 7.1 million tons of slag [18]. With the Vietnamese steel market projected to be one of the fastest-growing globally from 2020 to 2024, the volume of steel slag produced is expected to increase significantly [18]. In Vietnam, steel slag is primarily utilized in construction. However, the lack of specific guidelines and regulations for its application has led to a considerable portion of slag being stored in factory yards or buried rather than effectively utilized [18].

SS, rich in calcium, silica, aluminum, and iron oxides, is highly suitable for multiple applications, such as serving as ballast in concrete and acting as a sorbent for pollutants [17]. Numerous studies have explored its effectiveness in eliminating heavy metals from water. For instance, Liem Nguyen et al. investigated the adsorption of arsenic (As) using steel slag, achieving a capacity of 4.3 mg/g [17]. Similarly, Yang et al. demonstrated the effectiveness of steelmaking slag in removing Pb(II), Cu(II), and Cd(II), with removal efficiencies exceeding 85% [19].

However, research on using steel slag for Cr(VI) removal remains limited, especially in Vietnam. Leveraging steel slag waste to produce adsorbents for contaminant removal not only addresses the challenge of waste management but also contributes to environmental sustainability. In light of this, our study focused on evaluating the potential of steel slag for Cr(VI) adsorption from aqueous solutions. Key aspects such as the material's properties, the effects of pH, contact time, initial Cr(VI) concentration, as well as the kinetics and isotherms of the adsorption process, were comprehensively analyzed.

2. Materials and methods

2.1. Materials

Chemical reagents such as potassium dichromate ($K_2Cr_2O_7$), hydrochloric acid (HCl), and sodium hydroxide

(NaOH) were procured from Merck (Germany). A Cr(VI) stock solution (1000 mg/L) was prepared by dissolving 0.5657 g of $K_2Cr_2O_7$ in 200 mL of double-distilled water, and working solutions were diluted accordingly.

SS from the Thai Nguyen Iron and Steel Corporation (Vietnam) was thoroughly rinsed with tap water, followed by distilled water, to remove residual impurities. Subsequently, it was dried at 105°C for 48 hours and ground to obtain a fine powder (<45 µm). It was further washed twice with hot deionized water, air-dried for 24 hours, and stored in glass containers for experiments.

2.2. Characterization of steel slag

The surface morphology of SS and SS after Cr(VI) adsorption (referred to as SS and SS-Cr, respectively) was examined using a scanning electron microscope (SEM) (HITACHI S-4800). The crystal structures were characterized by X-ray diffraction (XRD) analysis on a D8 ADVANCE system, employing Cu Kα radiation (λ = 1.54 Å). To identify the functional groups in SS and SS-Cr, Fourier transform infrared spectroscopy (FTIR-6300) was performed across a spectral range of 400–4000 cm^{-1}.

2.3. Adsorption experiments

Batch adsorption experiments were conducted in 50 mL Erlenmeyer flasks containing 25 mL of Cr(VI) solution at varying initial concentrations. The pH of each solution was adjusted using 0.1 M HCl or NaOH before introducing the SS adsorbent. The flasks were tightly sealed and agitated at 120 rpm using a mechanical shaker (PH-2A, China). After the predetermined contact time, samples were filtered through Whatman No. 1 filter paper (pore size 11 µm), and the residual Cr(VI) concentration was measured using an inductively coupled plasma-optical emission spectrometer (ICP-OES)

The adsorption capacity of SS at any time t (q_t, mg/g) and at equilibrium (q_e, mg/g) was calculated using Eqs (1) and (2).

$$q_t = \frac{(C_o - C_t)V}{m} \quad (1)$$

$$q_e = \frac{(C_o - C_e)V}{m} \quad (2)$$

Where: C_0, C_t and C_e (mg/L) represent the initial, time-dependent, and equilibrium Cr(VI) concentration, respectively; V (L) is the solution volume, and m (g) is the mass of SS used.

2.4. Theoretical study of the adsorption process

In this study, the kinetic data of the adsorption process were evaluated using three commonly applied models: pseudo-first-order, pseudo-second-order, and Elovich models. These models provide insights into the adsorption mechanism, distinguishing between physical adsorption (pseudo-first-order), chemical adsorption (pseudo-second-order), and heterogeneous adsorption involving different activation energies (Elovich) [20]. The nonlinear equations representing these commonly applied models are presented as Eqs (3), (4), and (5), respectively [20]:

$$\ln(q_e - q_t) = \ln q_e - k_1 t \quad (3)$$

$$\frac{t}{q_t} = \frac{1}{k_2 q_e^2} + \frac{1}{q_e} t \quad (4)$$

$$q_t = \beta \ln(\alpha\beta t) \quad (5)$$

Where: q_t and q_e (mg/g) denote the adsorption capacity at time t (min) and at equilibrium, respectively; k_1 ($1/min$) and k_2 ($g/mg.min$) are the rate constants of the pseudo-first-order and pseudo-second-order models, respectively; α ($mg/g.min$) represents the initial adsorption rate, and β (g/mg) is a parameter related to the adsorption process in the Elovich model.

The Langmuir and Freundlich models were employed to study the adsorption isotherm. The Langmuir model assumes monolayer adsorption on a homogeneous surface, while the Freundlich model accounts for multilayer adsorption on a heterogeneous surface [21]. Comparing these models provides insights into the adsorption behavior of Cr(VI) onto steel slag. Their respective equations are presented as Eqs (6) and (7) [21]:

$$q_e = \frac{q_m K_L C_e}{1 + K_L C_e} \quad (6)$$

$$q_e = K_F C_e^{\frac{1}{n}} \quad (7)$$

Where: q_m and q_e (mg/g) represent the maximum and equilibrium adsorption capacities of Cr(VI) onto SS, respectively; C_e (mg/L) is the concentration of Cr(VI) in the solution; K_L (L/mg) is the Langmuir constant; K_F (mg/g) is the Freundlich constant and n is the adsorption intensity;

3. Results and discussion

3.1. Characteristic of adsorbent

The surface morphology and element composition of SS and SS-Cr were analyzed using SEM and EDS techniques. As shown in Figure 1a and 1c, the surface of SS-Cr exhibited greater porosity and roughness compared to SS. Moreover, EDS analysis (Figure 1b and 1d) revealed that the primary elements in SS were C, O, Si, Fe, Al, Mn, Ca, Mg, Na. After loading with Cr^{6+}, Cr was detected in SS-Cr at a concentration of 0.35%, confirming the successful adsorption of Cr^{6+} ions on the SS surface.

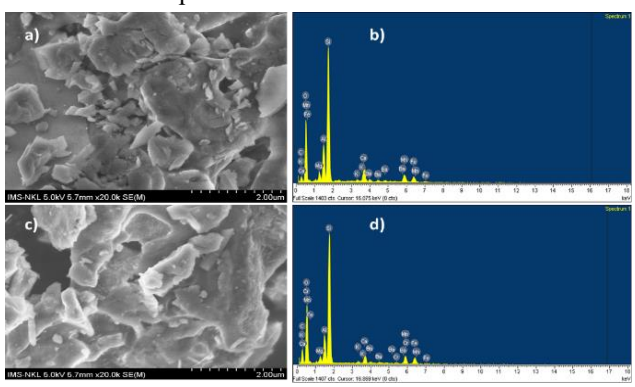

Figure 1. *SEM and EDS of (a, b)-steel slag (SS), (c, d) steel slag after Cr(VI) adsorption (SS-Cr)*

XRD analysis (Figure 2) showed distinct differences between SS and SS-Cr. SS exhibited peaks at 21.7°, 26.4°, and 49.4° corresponding to calcium silicate hydrate [22], along with hemicarbonate (31.1°) [23], $CaCO_3$ (35.4°, 36.4°, 37.9°) [22], mayenite (38.7°) [24], magnetite (44.4°, 65.3°) [25], quartz (59.8°, 67.9°) [26], and hematite (71.6°) [27]. After Cr^{6+} adsorption (SS-Cr), peak intensities decreased, with slight positional shifts. These changes suggest possible interactions between Cr(VI) and the steel

slag components, potentially involving surface complexation or ion exchange, leading to structural modifications in the material.

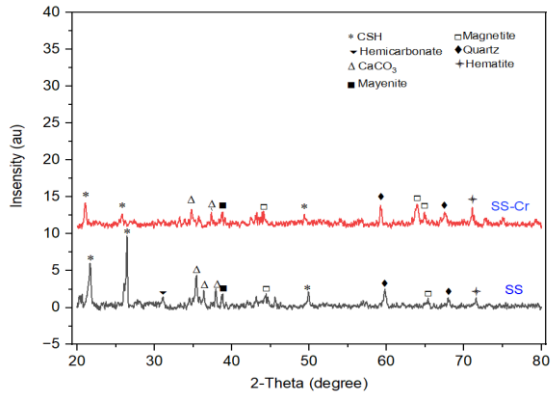

Figure 2. *XRD graphs of steel slag (SS) and steel slag after Cr(VI) adsorption (SS-Cr)*

To further investigate the structural features of SS and SS-Cr, Fourier Transform Infrared Spectroscopy (FTIR) measurements were performed, as shown in Figure 3.

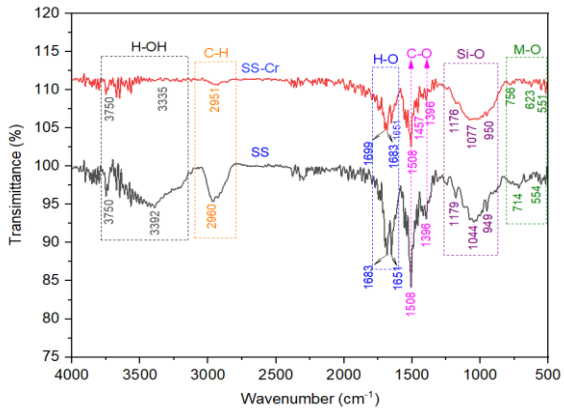

Figure 3. *FTIR spectra of steel slag (SS) and steel slag after Cr(VI) adsorption (SS-Cr)*

Both SS and SS-Cr exhibited weak peaks in the range of 551 cm^{-1} to 756 cm^{-1}, which can be attributed to various oxides (M-O), including Al_2O_3, Fe_2O_3, MgO, ferrites, and other metallic oxides [28]. The absorption bands between 949 cm^{-1} and 1176 cm^{-1} are characteristics of Si-O stretching modes of silica and silicates [29]. Additionally, absorption bands in this region may also correspond to hydroxyl vibrations of aluminum oxyhydroxides and iron oxyhydroxides [26, 27]. The adsorption bands for C-O stretching modes of the CO_3^{2-} ion were observed in the range of approximately 1396 cm^{-1} to 1508 cm^{-1} [30]. Bands appearing around 1651 cm^{-1} to 1699 cm^{-1} and 3335 cm^{-1} to 3750 cm^{-1} were assigned to the deformation modes of H-O vibrations [31]. Furthermore, a broad peak near 2960 cm^{-1} was attributed to the vibration of C–H stretching [32]. After SS adsorbed Cr^{6+}, notable changes were observed in the FTIR spectrum. The intensities of several peaks, such as those at 1396 cm^{-1}, 1508 cm^{-1}, 1683 cm^{-1}, 2960 cm^{-1}, 3392 cm^{-1}, and 3750 cm^{-1}, decreased compared to SS. Additionally, some peaks exhibited both a reduction in intensity and a shift in position. Specifically, the peaks at 714 cm^{-1}, 1044 cm^{-1}, 2960 cm^{-1}, 3392 cm^{-1} in SS were shifted to 756 cm^{-1}, 1077 cm^{-1}, 2951 cm^{-1}, 3335 cm^{-1} in SS-Cr. Moreover, new peaks were observed in SS-Cr at 1457 cm^{-1}, 1651 cm^{-1} and 1699 cm^{-1}. These spectral changes indicate that the adsorption of Cr^{6+} significantly altered the surface functional groups of SS [33].

3.2. Effects of adsorption conditions on SS performance

3.2.1. Effect of solution pH

The adsorption of Cr(VI) onto SS was significantly influenced by the initial pH of the solution, with experiments conducted at pH values ranging from 2 to 8 (Figure 4).

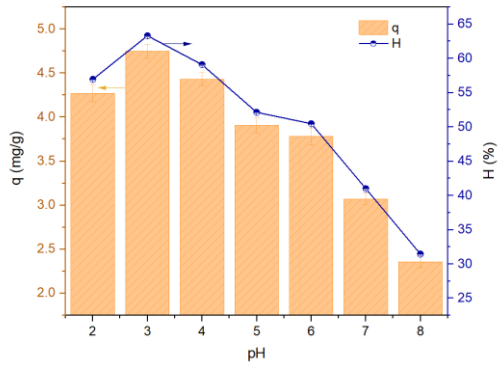

Figure 4. *Effect of initial solution pH on adsorption capacity and removal efficiency of Cr(VI) using SS. Experimental parameters: initial Cr(VI) concentrations of 20 mg/L; contact time of 60 min, and adsorbent dosage of 20 mg per 25 mL solution*

The results indicate that the adsorption of Cr(VI) onto SS was most efficient under acidic conditions, reaching maximum capacity and removal efficiency of 4.74 mg/g and 63.32 % at pH 3, respectively. Meanwhile, the Cr(VI) adsorption capacity and removal efficiency decreased significantly as the pH increased from 4 to 8. Under acidic conditions, Cr(VI) is readily reduced to Cr(III), which exhibits better adsorption properties compared to Cr(VI) [1]. Additionally, Cr(VI) primarily exists as $HCrO_4^-$ and $Cr_2O_7^{2-}$ at pH values ranging from 2.0 to 6.4, and as CrO_4^{2-} at pH > 6.4 [34]. Notably, $HCrO_4^-$ has lower adsorption-free energy (-2.5 to -0.6 kcal/mol) compared to CrO_4^{2-} (-2.1 to -0.3 kcal/mol) [34]. As a result, under identical conditions, CrO_4^{2-} is more challenging to remove than $HCrO_4^-$ [34]. Similar findings were reported by Wang et al, who found that a pH of 3.5 was optimal for the adsorption of Cr(VI) onto activated carbon [3], and Akram et al , who reported that the optimal pH for Cr(VI) adsorption onto a bio-composite derived from mango was also pH of 3 [35].

3.2.2. Effect of contact time and kinetic study

A series of experiments were conducted to evaluate the influence of contact time on Cr(VI) adsorption onto SS. As shown in Fig.5a, the adsorption capacity of Cr(VI) increased significantly during the first 60 minutes, followed by a gradual decline in the adsorption rate between 90 and 150 minutes. The maximum adsorption capacity and removal efficiency were observed at 150 minutes, reaching 6.13 mg/g and 81.75%, respectively. Beyond 150 minutes, the adsorption capacity remained constant. This trend can be attributed to the abundance of active sites on the adsorbent surface during the initial stage, which facilitated rapid adsorption [36]. Over time, as the

number of available active sites decreased, the adsorption process slowed and eventually reached equilibrium [36]. Therefore, 150 minutes was identified as the equilibrium time and was employed in subsequent experiments.

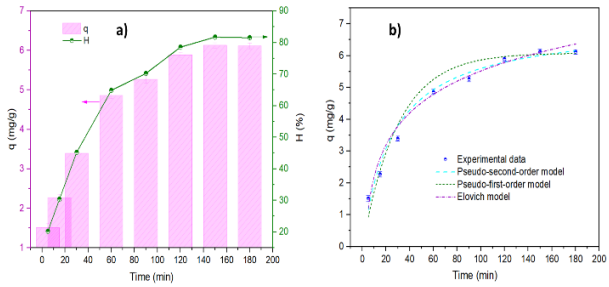

Figure 5. *(a) Effect of contact time on adsorption capacity and removal efficiency of Cr(VI) using SS. (b) Adsorption kinetics of Cr(VI) onto SS. Experimental parameters: initial Cr(VI) concentrations of 20 mg/L, the adsorbent dosage of 20 mg/25 mL, solution pH of 3.0, and contact times ranging 5–180 min*

Table 1. *Kinetics parameters of Cr(VI) adsorption models by SS*

Kinetic model	Kinetic parameters		$q_{e,\,exp}$ (mg/g)
Pseudo-first-order	$q_{e,\,cal}$ (mg/g)	6.08	6.13
	k_1	0.033	
	R^2	0.970	
Pseudo- second-order	$q_{e,\,cal}$ (mg/g)	7.02	
	k_2	0.005	
	R^2	0.985	
Elovich	α	0.319	
	β	1.442	
	R^2	0.971	

Three commonly used models, including the pseudo-first-order, pseudo-second-order and Elovich models, were applied to analyze the kinetics of Cr(VI) adsorption onto SS. The corresponding kinetic parameters are shown in Table 1 and Figure 5b. The linear regression coefficient (R^2) values for the pseudo-first-order, pseudo-second-order, and Elovich models were 0.970, 0.985, and 0.980, respectively, indicating that all three models exhibited a good fit. Among them, the pseudo-second-order model showed the highest R^2 value, suggesting it best describes the adsorption behavior [34]. Furthermore, the adsorption capacity predicted by the pseudo-second-order model (7.02 mg/g) closely matched the experimental value (6.13 mg/g). This demonstrates that the pseudo-second-order model most accurately describes the adsorption behavior of Cr(VI) onto SS and confirms that the process is dominated by chemical sorption, involving valence forces such as electron sharing or exchange [34]. These observations are consistent with trends reported in other studies on Cr(VI) adsorption [33, 34].

3.2.3. Effect of initial Cr(VI) concentration and isotherms

The adsorption capacity of SS for Cr(VI) was examined across an initial concentration range of 5–80 mg/L. The obtained data were fitted to the Langmuir and Freundlich isotherm models, with results in Table 2 and Figure 6.

As illustrated in Figure 6a, the adsorption capacity of SS for Cr(VI) increased from 1.80 mg/g to 11.87 mg/g as the initial Cr(VI) concentration rose from 5 to 60 mg/L. Beyond 60 mg/L, however, no further increase in adsorption capacity was observed. Conversely, the percentage of Cr(VI) removed decreased from 93.56% to 38.54% as the initial Cr(VI) concentration increased from 5 to 80 mg/L. This behavior can be attributed to the higher availability of active sites on the adsorbent surface at lower Cr(VI) concentrations, enabling effective adsorption. At higher concentrations, the active sites became saturated, limiting further adsorption [21]. Furthermore, the ratio of available active sites to Cr(VI) ions decreased at higher Cr(VI) concentrations, leading to a decline in removal efficiency [21]. A similar pattern regarding the influence of initial Cr(VI) concentration on adsorption has been documented in studies involving Cr(VI) removal using MnO_2 [39] and walnut hulls [40].

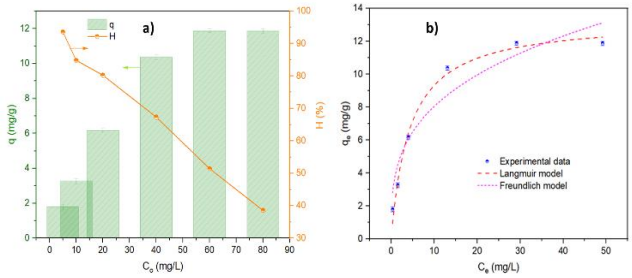

Figure 6. *(a) Effect of initial Cr(VI) concentration on the adsorption capacity and removal efficiency using SS. (b) Adsorption isotherms of Cr(VI) onto SS. Experimental parameters: initial Cr(VI) concentration ranging 5–80 mg/L, solution pH of 3.0, contact time of 150 min, and adsorbent dosage of 20 mg/25 mL*

Table 2. *The adsorption isothermal parameters of Cr(VI) onto SS*

Langmuir model			Freundlich model			q_{mexp} (mg/g)
q_m (mg/g)	K_L	R^2	K_F	1/n	R^2	11.87
13.32	0.233	0.986	3.968	0.307	0.905	

The Langmuir model was identified as the most suitable for describing the adsorption of Cr(VI) onto SS, based on its highest R^2 value (0.986) and the close agreement between the calculated q_m value (13.32 mg/g) and experimental q_{exp} value (11.87 mg/g). This indicates that the adsorption predominantly occurred as a monolayer or through a fixed number of uniform adsorption sites on the SS surface. Additionally, the adsorption process took place at homogeneous adsorption sites on the SS adsorbent [36]. Moreover, the 1/n value (0.307) derived from the Freundlich model was less than 1, suggesting that the adsorption of Cr(VI) onto SS is favorable [10].

3.2.4. Adsorption mechanism of the Cr(VI) ions onto SS

Adsorption isotherms, kinetics, and mechanisms offer crucial insights into the underlying reaction pathways. In this study, the adsorption of Cr(VI) onto steel slag (SS) may involve four primary mechanisms: (1) pore filling, (2) adsorption-coupled reduction, (3) electrostatic attraction, and (4) electron sharing or exchange.

As shown in Figure 1, the SEM images revealed that after Cr(VI) adsorption, the steel slag surface (SS-Cr) exhibited increased porosity and roughness. This suggests that Cr(VI) may be physically retained within the pores of SS, contributing to its removal from the solution.

The pH-dependent adsorption analysis indicated that Cr(VI) adsorption was most effective under acidic

conditions. During this process, Cr(VI) was initially reduced to Cr(III) upon interaction with electron-donor groups on the SS surface [41]. FTIR analysis (Figure 3) revealed a decrease in the intensity of carboxyl (-COO^-) and hydroxyl (-OH) functional groups at 1396 cm^{-1}, 1508 cm^{-1}, and 1651–1699 cm^{-1}, suggesting their involvement in Cr(VI) reduction. Additionally, Fe^{2+} present in SS may have been oxidized to Fe^{3+}, further facilitating the reduction of Cr(VI) to Cr(III) [42]. Once reduced, Cr(III) was adsorbed onto SS via three possible pathways: (i) substitution of Fe^{3+} with Cr^{3+} under acidic conditions, (ii) complexation with surface functional groups, and (iii) precipitation as $Cr(OH)_3$ [21]. The XRD patterns indicated changes in the crystal structure of SS after Cr(VI) adsorption, while EDS analysis detected Cr on the SS surface, verifying its adsorption.

Electrostatic interactions also played a role in Cr(VI) adsorption [43]. Under acidic conditions, functional groups on the SS surface may become protonated, enhancing interactions with Cr(VI) species [1]. Additionally, adsorption could occur due to charge imbalances, vacancy sites, and chemical bonding with magnetite (Fe_3O_4) and hematite (Fe_3O_4) present on the SS surface [43].

Adsorption kinetics and isotherm analyses (Sections 3.2.2 and 3.2.3) indicated that the adsorption process involved electron sharing or exchange between Cr(VI) and active sites on SS, which contributed to adsorption stability. This suggests that Cr(VI) adsorption onto SS followed a homogeneous adsorption mechanism, where electron transfer played a role in binding Cr(VI) to the SS surface. This mechanism is consistent with previous studies [33, 34, 36].

Table 3. *Comparison of SS adsorption capacity toward Cr(VI) in aqueous solution with other adsorbents*

Adsorbent	Equilibrium Cr(VI) concentration range (mg/L)	Langmuir maximum adsorption capacity (mg/g)	References
Steel slag (SS)	5-80	13.32	This study
Fly ash-based geopolymer adsorbent (FAGA)	20-120	49.75	[15]
Furnace slag (FS)	-	4.83	[11]
Magnetic nanoparticles (Fe_3O_4) capped with cetyltrimethylammoniumbromide (Fe_3O_4/CTAB)	10 - 200	18.5	[46]
Mechanical-chemical activated red mud (MCARM)	5-200	6.7	[47]

To assess the Cr(VI) adsorption capacity of SS, the results of this study were compared with those from other reports, as presented in Table 3. The data in Table 3 show that the Cr(VI) adsorption capacity of SS was lower than that of fly ash-based geopolymer adsorbent (FAGA) [15] and magnetic nanoparticles (Fe_3O_4) capped with cetyltrimethylammonium bromide (Fe_3O_4/CTAB) [46]. However, it was higher than that of furnace slag (FS) and mechanically-chemically activated red mud (MCARM). These findings indicate that SS is an economical adsorbent with promising efficiency for Cr(VI) removal from aqueous solutions.

4. Conclusion

This study demonstrated that steel slag (SS) is a promising adsorbent for Cr(VI) removal from aqueous solutions due to its cost-effectiveness and efficient performance. The adsorption process reached equilibrium within 150 minutes, with the highest adsorption capacity observed at a pH of 3.0. The findings indicate that increasing the SS dosage and extending the contact time enhanced Cr(VI) removal efficiency. The maximum adsorption capacity, as determined by the Langmuir model, was 13.32 mg/g at an initial Cr(VI) concentration of 20 mg/L. Kinetic and isotherm analyses indicated that the pseudo-second-order kinetic model and Langmuir isotherm best described the adsorption behavior. The removal of Cr(VI) by steel slag occurred through a combination of four key mechanisms: physical entrapment within the material's pores, reduction-assisted adsorption, electrostatic interactions, and electron exchange or sharing at active sites. These mechanisms collectively contribute to the effective adsorption performance of steel slag.

Although pH 3 facilitated optimal Cr(VI) removal, the potential dissolution of metal ions from SS, particularly Fe, Ca, and Al, under acidic conditions should be considered. This study primarily focused on the adsorption performance of SS, and further research is needed to assess the stability of SS in acidic environments. Future studies should explore potential modifications to the material to minimize unwanted metal leaching while maintaining its adsorption efficiency for Cr(VI).

Acknowledgements: We would like to express our sincere gratitude to the Thai Nguyen University of Technology for providing the necessary facilities, equipment, and research environment that greatly contributed to the successful completion of this study.

REFERENCES

[1] C. Lin, W. Luo, T. Luo, Q. Zhou, H. Li, and L. Jing, "A study on adsorption of Cr (VI) by modified rice straw: Characteristics, performances and mechanism", *J. Clean. Prod.*, vol. 196, no. Vi, pp. 626–634, 2018, doi: 10.1016/j.jclepro.2018.05.279.

[2] WHO, "Chromium in Drinking-water Background document for development of WHO Guidelines for Drinking-water Quality", 1996.

[3] Y. Wang, C. Peng, E. Padilla-Ortega, A. Robledo-Cabrera, and A. López-Valdivieso, "Cr(VI) adsorption on activated carbon: Mechanisms, modeling and limitations in water treatment", *J. Environ. Chem. Eng.*, vol. 8, no. 4, 2020, doi: 10.1016/j.jece.2020.104031.

[4] Y. Fei and Y. H. Hu, "Design, synthesis, and performance of adsorbents for heavy metal removal from wastewater: a review", *J. Mater. Chem. A*, vol. 10, no. 3, pp. 1047–1085, 2022, doi: 10.1039/D1TA06612A.

[5] A. Mohammadi, A. Ataie, and S. Sheibani, "Chromium (VI) Ions Adsorption Onto Barium Hexaferrite Magnetic Nano-adsorbent", *Adv. Mater. Lett.*, vol. 7, no. 7, pp. 579–586, 2016, doi: 10.5185/amlett.2016.6394.

[6] K. S. Padmavathy, G. Madhu, and P. V Haseena, "A study on Effects of pH, Adsorbent Dosage, Time, Initial Concentration and Adsorption Isotherm Study for the Removal of Hexavalent Chromium (Cr (VI)) from Wastewater by Magnetite Nanoparticles", *Procedia Technol.*, vol. 24, pp. 585–594, 2016, doi: https://doi.org/10.1016/j.protcy.2016.05.127.

[7] H. Wang *et al.*, "Facile synthesis of polypyrrole decorated reduced graphene oxide–Fe_3O_4 magnetic composites and its application for the Cr(VI) removal", *Chem. Eng. J.*, vol. 262, pp. 597–606, 2015, doi: https://doi.org/10.1016/j.cej.2014.10.020.

[8] D. K. Grgić, "Batch Adsorption of Cr(VI) Ions on Zeolite and Agroindustrial Waste", *Chem. Biochem. Eng. Q.*, vol. 31, pp. 497–507, Jan. 2018, doi: 10.15255/CABEQ.2017.1100.

[9] A. Tytłak, P. Oleszczuk, and R. Dobrowolski, "Sorption and desorption of Cr(VI) ions from water by biochars in different environmental conditions", *Environ. Sci. Pollut. Res.*, vol. 22, no. 8, pp. 5985–5994, 2015, doi: 10.1007/s11356-014-3752-4.

[10] H. Wang, W. Wang, S. Zhou, and X. Gao, "Adsorption mechanism of Cr(VI) on woody-activated carbons", *Heliyon*, vol. 9, no. 2, p. e13267, 2023, doi: https://doi.org/10.1016/j.heliyon.2023.e13267.

[11] T. C. Nguyen, P. Loganathan, T. V. Nguyen, J. Kandasamy, R. Naidu, and S. Vigneswaran, "Adsorptive removal of five heavy metals from water using blast furnace slag and fly ash.", *Environ. Sci. Pollut. Res. Int.*, vol. 25, no. 21, pp. 20430–20438, Jul. 2018, doi: 10.1007/s11356-017-9610-4.

[12] V. K. Gupta and S. Sharma, "Removal of Cadmium and Zinc from Aqueous Solutions Using Red Mud", *Environ. Sci. Technol.*, vol. 36, no. 16, pp. 3612–3617, Aug. 2002, doi: 10.1021/es020010v.

[13] Pranoto, A. Masykur, and Y. A. Nugroho, "Adsorption Effectivity Test of Andisols Clay-Zeolite (ACZ) Composite as Chromium Hexavalent (Cr(VI)) Ion Adsorbent", *IOP Conf. Ser. Mater. Sci. Eng.*, vol. 333, no. 1, p. 12057, 2018, doi: 10.1088/1757-899X/333/1/012057.

[14] J. Liu, X. Wu, Y. Hu, C. Dai, Q. Peng, and D. Liang, "Effects of Cu(II) on the Adsorption Behaviors of Cr(III) and Cr(VI) onto Kaolin", *J. Chem.*, vol. 2016, no. Vi, 2016, doi: 10.1155/2016/3069754.

[15] J. Qiu, Y. Zhao, J. Xing, and X. Sun, "Fly ash-based geopolymer as a potential adsorbent for Cr(VI) removal", *Desalin. Water Treat.*, vol. 70, pp. 201–209, 2017, doi: https://doi.org/10.5004/dwt.2017.20493.

[16] N. Sheraz, A. Shah, A. Haleem, and F. J. Iftikhar, "Comprehensive assessment of carbon-, biomaterial- and inorganic-based adsorbents for the removal of the most hazardous heavy metal ions from wastewater", *RSC Adv.*, vol. 14, no. 16, pp. 11284–11310, 2024.

[17] V. Liem-Nguyen, V. Sjöberg, N. P. Dinh, D. H. Huy, and S. Karlsson, "Removal mechanism of arsenic (V) by stainless steel slags obtained from scrap metal recycling", *J. Environ. Chem. Eng.*, vol. 8, no. 4, p. 103833, 2020, doi: 10.1016/j.jece.2020.103833.

[18] L. H. Nguyen *et. al.*, "Steel slag quality control for road construction aggregates and its environmental impact: case study of Vietnamese steel industry-leaching of heavy metals from steel-making slag", *Environ. Sci. Pollut. Res.*, vol. 29, no. 28, pp. 41983–41991, 2022, doi: 10.1007/s11356-021-16438-1.

[19] L. Yang *et. al.*, "The stability of the compounds formed in the process of removal Pb(II), Cu(II) and Cd(II) by steelmaking slag in an acidic aqueous solution", *J. Environ. Manage.*, vol. 231, no. September 2018, pp. 41–48, 2019, doi: 10.1016/j.jenvman.2018.10.028.

[20] T. M. Vu *et. al.*, "High removal efficiency of ammonium from aqueous solution by colloidal silver nanoparticles: batch adsorption", *Urban Water J.*, vol. 21, no. 3, pp. 323–336, 2024, doi: 10.1080/1573062X.2023.2290614.

[21] H. L. Phuong *et. al.*, "Removal of Cr(vi) from aqueous solution using magnetic modified biochar derived from raw corncob", *New J. Chem.*, vol. 43, no. 47, pp. 18663–18672, 2019, doi: 10.1039/C9NJ02661D.

[22] W. Hunnicutt, "Characterization of calcium-silicate-hydrate and calcium-alumino-silicate-hydrate", University of Illinois at Urbana-Champaign, 2013.

[23] N. Shao, S. Li, F. Yan, Y. Su, F. Liu, and Z. Zhang, "An all-in-one strategy for the adsorption of heavy metal ions and photodegradation of organic pollutants using steel slag-derived calcium silicate hydrate", *J. Hazard. Mater.*, vol. 382, no. August 2019, p. 121120, 2020, doi: 10.1016/j.jhazmat.2019.121120.

[24] I. Z. Yildirim and Monica Prezzi, "Steel Slag: Chemistry, Mineralogy, and Morphology", pp. 2816–2825, 2015.

[25] L.S. Rocha *et. al.*, "Producing Magnetic Nanocomposites from Paper Sludge for the Adsorptive Removal of Pharmaceuticals from Water-A Fractional Factorial Design", *Nanomaterials*, vol. 11, pp. 1–20, Jan. 2021, doi: 10.3390/nano11020287.

[26] R. F. Zuo, G. X. Du, W. G. Yang, L. B. Liao, and Z. Li, "Mineralogical and chemical characteristics of a powder and purified quartz from Yunnan Province", *Open Geosci.*, vol. 8, no. 1, pp. 606–611, 2016, doi: 10.1515/geo-2016-0055.

[27] R. Wahab, F. Khan, and A. A. Al-Khedhairy, "Hematite iron oxide nanoparticles: apoptosis of myoblast cancer cells and their arithmetical assessment", *RSC Adv.*, vol. 8, no. 44, pp. 24750–24759, 2018, doi: 10.1039/C8RA02613K.

[28] C. Navarro, M. Díaz, and M. A. Villa-García, "Physico-chemical characterization of steel slag. study of its behavior under simulated environmental conditions", *Environ. Sci. Technol.*, vol. 44, no. 14, pp. 5383–5388, 2010, doi: 10.1021/es100690b.

[29] N. Shao *et al.*, "Hierarchically Structured Calcium Silicate Hydrate-Based Nanocomposites Derived from Steel Slag for Highly Efficient Heavy Metal Removal from Wastewater", *ACS Sustain. Chem. Eng.*, vol. 6, no. 11, pp. 14926–14935, 2018, doi: 10.1021/acssuschemeng.8b03428.

[30] S. Wang, X. Peng, L. Tang, L. Zeng, and C. Lan, "Influence of inorganic admixtures on the 11 Å-tobermorite formation prepared from steel slags: XRD and FTIR analysis", *Constr. Build. Mater.*, vol. 60, pp. 42–47, 2014, doi: 10.1016/j.conbuildmat.2014.03.002.

[31] Y. L. Lee, W. H. Wang, F. H. Lin, and C. P. Lin, "Hydration behaviors of calcium silicate-based biomaterials", *J. Formos. Med. Assoc.*, vol. 116, no. 6, pp. 424–431, 2017, doi: 10.1016/j.jfma.2016.07.009.

[32] M.S. Tizo *et. al.*, "Efficiency of calcium carbonate from eggshells as an adsorbent for cadmium removal in aqueous solution", *Sustain. Environ. Res.*, vol. 28, no. 6, pp. 326–332, 2018, doi: https://doi.org/10.1016/j.serj.2018.09.002.

[33] G. K. Gupta, M. Ram, R. Bala, M. Kapur, and M. K. Mondal, "Pyrolysis of chemically treated corncob for biochar production and its application in Cr(VI) removal", *Environ. Prog. Sustain. Energy*, vol. 37, no. 5, pp. 1606–1617, 2018, doi: 10.1002/ep.12838.

[34] J. Shang, J. Pi, M. Zong, Y. Wang, W. Li, and Q. Liao, "Chromium removal using magnetic biochar derived from herb-residue", *J. Taiwan Inst. Chem. Eng.*, vol. 68, pp. 289–294, 2016, doi: https://doi.org/10.1016/j.jtice.2016.09.012.

[35] M. Akram, H. N. Bhatti, M. Iqbal, S. Noreen, and S. Sadaf, "Biocomposite efficiency for Cr(VI) adsorption: Kinetic, equilibrium and thermodynamics studies", *J. Environ. Chem. Eng.*, vol. 5, no. 1, pp. 400–411, 2017, doi: https://doi.org/10.1016/j.jece.2016.12.002.

[36] H. L. Phuong *et. al.*, "Cr(VI) Removal from Aqueous Solution Using a Magnetite Snail Shell", *Water, Air, Soil Pollut.*, vol. 231, no. 1, p. 28, 2020, doi: 10.1007/s11270-020-4406-4.

[37] Y. Yang, N. Chen, C. Feng, M. Li, and Y. Gao, "Chromium removal using a magnetic corncob biochar/polypyrrole composite by adsorption combined with reduction: Reaction pathway and contribution degree", *Colloids Surfaces A Physicochem. Eng. Asp.*, vol. 556, pp. 201–209, 2018, doi: https://doi.org/10.1016/j.colsurfa.2018.08.035.

[38] Y. Chen, B. Wang, J. Xin, P. Sun, and D. Wu, "Adsorption behavior and mechanism of Cr(VI) by modified biochar derived from Enteromorpha prolifera", *Ecotoxicol. Environ. Saf.*, vol. 164, pp. 440–447, 2018, doi: https://doi.org/10.1016/j.ecoenv.2018.08.024.

[39] M. Gheju, I. Balcu, and G. Mosoarca, "Removal of Cr(VI) from aqueous solutions by adsorption on MnO2", *J. Hazard. Mater.*, vol. 310, no. Vi, pp. 270–277, 2016, doi: 10.1016/j.jhazmat.2016.02.042.

[40] X. S. Wang, Z. Z. Li, and S. R. Tao, "Removal of chromium (VI) from aqueous solution using walnut hull", *J. Environ. Manage.*, vol. 90, no. 2, pp. 721–729, 2009, doi: https://doi.org/10.1016/j.jenvman.2008.01.011.

[41] H. N. Tran *et al.,* "Adsorption mechanism of hexavalent chromium onto layered double hydroxides-based adsorbents: A systematic in-depth review", *Journal of Hazardous Materials*, vol. 373, pp. 258-270, 2019. https://doi.org/10.1016/j.jhazmat.2019.03.018

[42] X. He, X. Qiu, and J. Chen, "Preparation of Fe (II)– Al layered double hydroxides : Application to the adsorption / reduction of chromium", vol. 516. Colloids and Surfaces A: Physicochemical and Engineering Aspects, pp. 362–374, 2017.

[43] Q. An, X. Q. Li, H. Y. Nan, Y. Yu, and J. N. Jiang, "The potential adsorption mechanism of the biochars with different modification processes to Cr(VI)", *Environ. Sci. Pollut. Res.*, vol. 25, no. 31, pp. 31346–31357, 2018, doi: 10.1007/s11356-018-3107-7.

[44] C. Yang, J. Yuan, Y. Guo, and X. Luo, "In situ nano-assembly of Mg/Al LDH embedded on phosphorylated cellulose microspheres for tetracycline hydrochloride removal", *Cellulose*, vol. 28, no. 1, pp. 301–316, 2021, doi: 10.1007/s10570-020-03533-8.

[45] A. Zaher, M. Taha, and R. K. Mahmoud, "Possible adsorption mechanisms of the removal of tetracycline from water by La-doped Zn-Fe-layered double hydroxide", *J. Mol. Liq.*, vol. 322, no. xxxx, p. 114546, 2021, doi: 10.1016/j.molliq.2020.114546.

[46] S. A. Elfeky, S. E. Mahmoud, and A. F. Youssef, "Applications of CTAB modified magnetic nanoparticles for removal of chromium (VI) from contaminated water", *J. Adv. Res.*, vol. 8, no. 4, pp. 435–443, 2017, doi: https://doi.org/10.1016/j.jare.2017.06.002.

[47] N. Ghanbarpourabdoli, S. Raygan, and H. Abdizadeh, "Investigating selective removal of Cr(VI) and Zinc ions from aqueous media by mechanical-chemical activated red mud", *IUST*, vol. 13, no. 4, pp. 20–32, Dec. 2016, doi: 10.22068/ijmse.13.4.20.